Integrating sulfur-doped atomic-dispersed FeN_x sites with small-sized Fe_3C nanoparticles for PEMFCs and Beyond

Chao Liu[ab], Jie Zheng[a], Bin Chi[c], Chengzhi Zhong[c], YingJie Deng[a], Chao Chen[a], Dai Dang[ab]*, Wenjun Fan[d]*, Zhiming Cui[c]*, Quanbing Liu[ab]*

a School of Chemical Engineering and Light Industry, Guangdong Provincial Key Laboratory of Plant Resources Biorefinery, Guangdong University of Technology, Guangzhou, China, 510006.

b Guangdong Provincial Laboratory of Chemistry and Fine Chemical Engineering Jieyang Center, Jieyang 515200, China

c The Key Laboratory of Fuel Cell Technology of Guangdong Province, School of Chemistry and Chemical Engineering, South China University of Technology, Guangzhou, 510641, China;

d State Key Laboratory of Catalysis, iChEM, Dalian Institute of Chemical Physics, Chinese Academy of Sciences, Dalian 116023, China

*Corresponding author E-mail address: *Dai Dang (dangdai@gdut.edu.cn), Wenjun Fan (wjfan@dicp.ac.cn), Zhiming Cui (zmcui@scut.edu.cn) and Quanbing Liu (liuqb@gdut.edu.cn)*

Table of contents

1. Experimental section

1.1 Chemicals

Ferric acetylacetonate, thiourea, and melamine were purchased from Shanghai Chemical Reagent Plant, China. All aqueous solution was prepared with high-purity de-ionized water (DI-water, resistance 18.2 MΩ cm^{-1}). All reagents were analytical grade and used without further purification.

1.2 Preparation of Fe-S-NC/Fe_3C catalysts

Melamine and iron acetylacetone were mixed with a mass ratio of 4:1, and then thiourea accounted for 11 wt% of the total mass was added into the above mixture to grind together into fine powder. The mixture was allowed to completely dry at room temperature. The resulting uniform admixture was placed into an alumina combustion boat, then the boat was put at the center of a horizontal quartz tube furnace and subjected to a temperature-programmed reaction. The mixture was firstly annealed under a flowing argon atmosphere at 550 °C for 1 h, at heating rate of 2 °C min^{-1}, then pyrolyzed at 850 °C for 1 h, at heating rate of 5 °C min^{-1}. The obtained material was then cooled naturally to room temperature under the protection of Ar atmosphere. After completing the pyrolysis reaction and cooling down, the obtained black material was ground into fine powder and treated with 0.5 M H_2SO_4 at 80°C for 8 hours, centrifuged overnight to dry, and further calcined at 850℃ in Ar atmosphere for 1 hour. The resulting catalysts were labeled as Fe-S-X, where X is the thiourea relative doping amount versus the precursor. The material with the optimal S doping amount is referred as Fe-S-11, which is named as Fe-S-NC/Fe_3C in the text. For comparison, the Fe-NC/Fe_3C (Fe-S-0) was prepared with the same protocol except for the absence of S

element. The synthesis steps for Fe-NC are almost identical to those of Fe-NC/Fe_3C, except that the iron acetylacetonate content is reduced by a factor of 10.

1.3 Characterizations

Raman spectra were obtained from 500 to 2000 cm^{-1} on a Raman spectrometer (LabRAM HR, HORIBA). X-ray diffraction (XRD) patterns were obtained at the 2θ angle of 5 to 80° at a scan rate of 5° min^{-1} by using Cu Kα radiation (λ = 0.15418 nm) on a Rigaku D/max 2500 X-ray diffractometer. X-ray photoelectron spectroscopy (XPS) was conducted on a VG ESCALAB MK2 X-ray photoelectron spectrometer (VG Corporation, UK) using an Al-Kα X-ray source. Low-pressure N_2 adsorption–desorption isotherms for the Brunauer–Emmett–Teller (BET) specific surface area was recorded on an Autosorb-iQ (Quantachrome) analyzer at 77 K. The morphologies of the samples were investigated by using a scanning electron microscope (SEM FEI Nova™ NanoSEM230). Transmission electron microscopy (TEM) and high-angle annular dark-field scanning TEM (HAADF-STEM) were performed by a JEM-2200FS instrument (JEOL, Japan) at an operating voltage of 200 kV. Samples were prepared for imaging by dispersing the catalyst powder in ultrapure ethanol and sonicating for 1 h, followed by dropping the suspension onto a carbon microgrid made from a 300 mesh copper grid. X-ray absorption fine structure (XAFS) spectra was recorded on the BL14W beamline at the Shanghai Synchrotron Radiation Facility (SSRF), Shanghai Institute of Applied Physics, China. The powder catalysts were characterized in transmission mode, and the energy of Fe K-edge were calibrated using standard Fe foil. The XAFS raw data were background-subtracted and normalized by the ATHENA program.

1.4 Evaluation of catalysts

Electrocatalytic activity measurements were conducted on an Ivium electrochemical workstation at room temperature, using a standard three-electrode system. The glassy carbon (GC) electrode (0.196 cm^{-2}) was used as the working electrode, and graphite rods was used as the counter electrode. An Ag/AgCl (3 M KCl solution) reference electrode was used in the acidic medium, and a Hg/HgO (1 M KOH solution) reference

electrode was used in the alkaline medium.

The working electrode was prepared as follows: 5 mg as synthesized catalyst was dispersed in 1 mL Nafion/ethanol (0.25 wt.% Nafion) under sonication for 30 min. Then, 20 μL of the dispersion was loaded on a GC electrode and dried under infrared illumination. The catalyst load was approximately 500 μg cm^{-2}.

Catalyst linear scanning voltammetry (LSV) tests and cyclic voltammetry (CV) were performed in 0.1 M KOH and 0.1 M $HClO_4$ electrolytes of O_2 or N_2 at a scan rate of 10 mV s^{-1}. Durability testing was conducted at 0.60 V for 12 h at a rotation rate of 1600 rpm in an O_2 saturated 0.1 M KOH solution and an O_2 saturated 0.1M $HClO_4$ solution, using the chronoamperometric technique.

Catalyst charge transfer numbers, hydrogen peroxide (H_2O_2) yields and electron transfer numbers were obtained from the results of rotating ring-disk electrode (RRDE) tests. The RRDE was also calculated by linear scanning voltammetry (LSV) in O_2-saturated 0.1 M KOH and 0.1 M $HClO_4$ solutions. The tests were performed in the scanning voltage range of −0.8 V to 0.2 V (for Hg/HgO) and 0.8 V to −0.2 V (for Ag/AgCl), respectively, at a scanning rate of 10 mV s^{-1} and a speed of 1600 rpm, while the ring electrode voltage was kept at 1.2 V vs RHE (0.1 M KOH) 1.3 V vs RHE (0.1 M $HClO_4$). The H_2O_2 yield was calculated by the following equation.

$$H_2O_2\ (\%) = (200 I_{ring}/N)/ (I_{disk} + (I_{ring}/N)) \quad (1)$$

The charge transfer number is calculated by the following equation.

$$n = (4 I_{disk})/ (I_{disk} + (I_{ring}/N)) \quad (2)$$

I_{ring} and I_{disk} are the absolute values of the ring and disk currents obtained during the test, respectively, and N is the collection efficiency, here the N is 0.37.

1.5 MEA preparation and fuel cell test

The single fuel cell performance of the cathode catalysts was evaluated in PEMFCs. The catalyst, isopropanol, and 5 wt.% Nafion ionomer solution (DuPont, USA) were ultrasonically mixed for 1 h. Then, the ink was sprayed on one side of a Nafion membrane (Gore, USA) using the catalyst sprayed membrane method, and the thickness of the membrane was 15.8 μm; the anode catalyst ink was prepared by the

same method using commercial 20% Pt/C (TKK, Japan) and sprayed on the other side of the membrane. The weight ratios for dry Nafion and catalyst are 1: 2 and 1: 2.5 on the cathode and anode catalyst layers, respectively. The catalyst loadings at the cathode were 3 mg cm^{-2}, and the Pt loading at the anode was 0.1 mg cm^{-2}. A control MEA of the Pt/C catalyst was prepared in the similar way with 0.2 mg_{Pt} cm^{-2} Pt/C (20%, TKK, Japan) as the cathode catalyst and 0.1 mg_{Pt} cm^{-2} Pt/C (20%, TKK, Japan) as the anode catalyst. A single fuel cell was assembled with the as prepared MEAs, with an area of 4.0 cm^2 and gas diffusion layers on both the sides. Fuel cell polarization plots were recorded using fuel cell test stations (Sunlaite, China). The fuel cell backpressure was 1 bar on both sides and the temperature was 70 °C. The flow rates of H_2, O_2, and air were 400, 600, and 800 mL min^{-1}, respectively.

1.6 Liquid Zinc-air battery tests

The catalyst inks were prepared by dispersed 1.0 mg catalyst in 1 mL of isopropyl alcohol with 5 wt.% Nafion as a binder by sonicating for 30 min. For the Zn-air battery test, the air electrode was prepared by uniformly coating the as-prepared catalyst ink onto carbon paper then drying it at 80 °C for 2 h. The mass loading was 1 mg cm^{-2} unless otherwise noted. A Zn foil was used as the anode and catalysis loaded on carbon paper are used as cathodes. Both electrodes were assembled into a home-made Zn-air battery, and 6 M KOH was used as the electrolyte to ensure reversible zinc electrochemical reactions at the anode. The polarization curves were recorded by linear sweep voltammetry (5 mV s^{-1}, at room temperature) on an Ivium electrochemical platform. The specific capacity and energy density are calculated from the galvanostatic discharge results, normalized to the mass of consumed Zn. The mass of consumed Zn is determined by the mass difference between the fresh Zn and resultant anode after discharging.

1.7 Computational Section.

All calculations were carried out using the Vienna Ab initio Simulation Package (VASP). The projector augmented wave (PAW) method was applied to treat electron–

ion interactions, and the Perdew-Burke-Ernzerhof (PBE) exchange–correlation functional within the generalized gradient approximation (GGA) was employed to describe the electron interactions. 520 eV cut-off energy was used in all simulations while the convergence threshold for the self-consistent field (SCF) and ion steps were set to be 1×10^{-5} eV and 0.02 eV $Å^{-1}$, respectively. The vacuum space of all investigated slab models was set to be 20 Å to avoid the interaction between periodic slabs. For structure optimization 3 × 3 × 1 Gamma-centred Monkhorst-Pack sampled k-points were used. The Gibbs free energies of the intermediates were calculated as $\Delta G = \Delta E + \Delta ZPE - T\Delta S$ at room temperature. The ΔE is the DFT-derived adsorption energy, which is the energy difference of configuration after and before adsorbed a reaction species. The ΔZPE and ΔS is the difference of zero point energy and the difference of entropy obtained by means of the harmonic approximation.

Supplementary Figures S1-S26 and Tables S1-S8

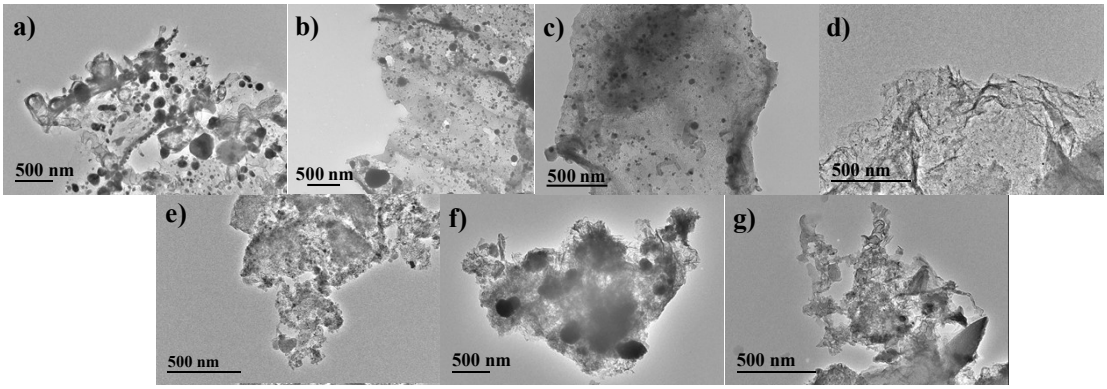

Figure S1. TEM images of Fe-S-0 (a), Fe-S-2 (b), Fe-S-6 (c), Fe-S-11 (d), Fe-S-16 (e), Fe-S-28 (f) and Fe-S-50 (g) catalysts by different ratios of S doping.

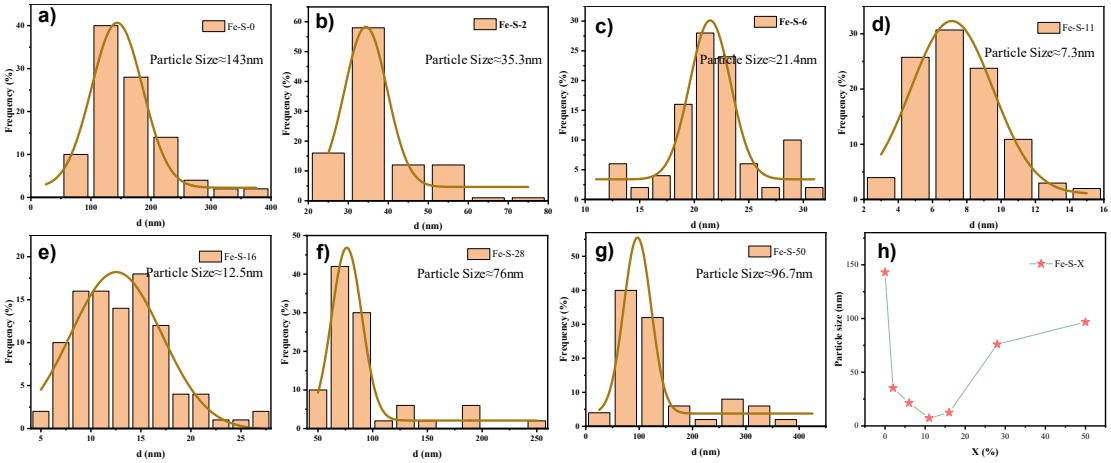

Figure S2. Particle size distribution (a-g) and trend graphs (h) for varying S doping levels.

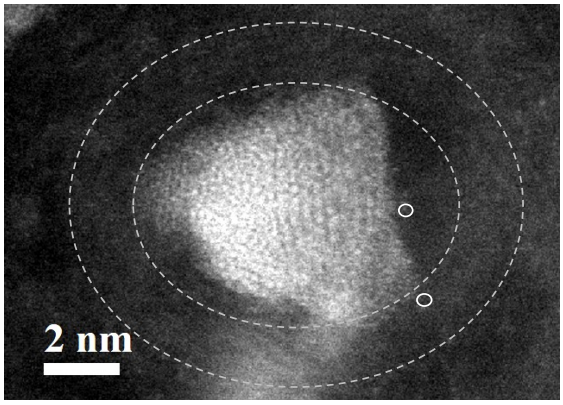

Figure S3. Atomic-resolution HAADF-STEM image of Fe-S-NC/Fe_3C.

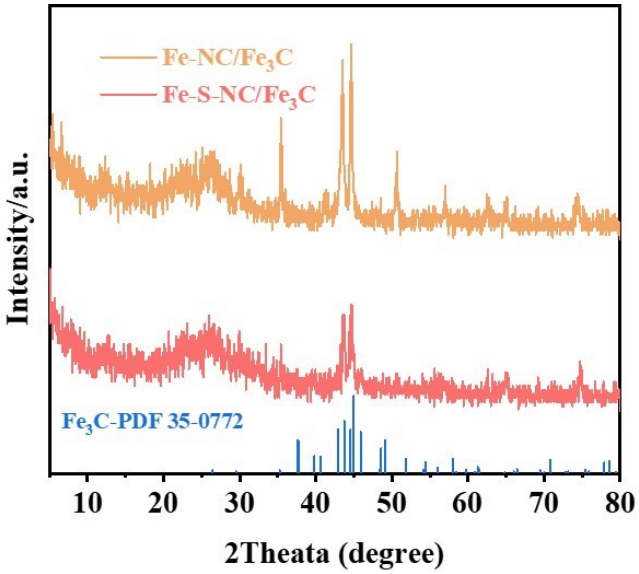

Figure S4. XRD patterns of Fe-S-NC/Fe_3C and Fe-NC/Fe_3C.

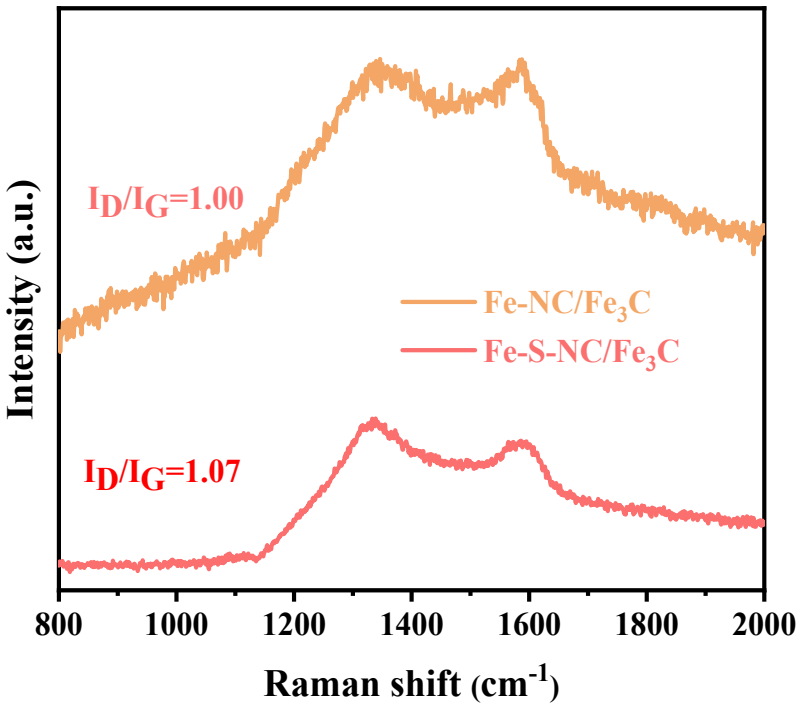

Figure S5. Raman scattering spectra of Fe-S-NC/Fe_3C and Fe-NC/Fe_3C.

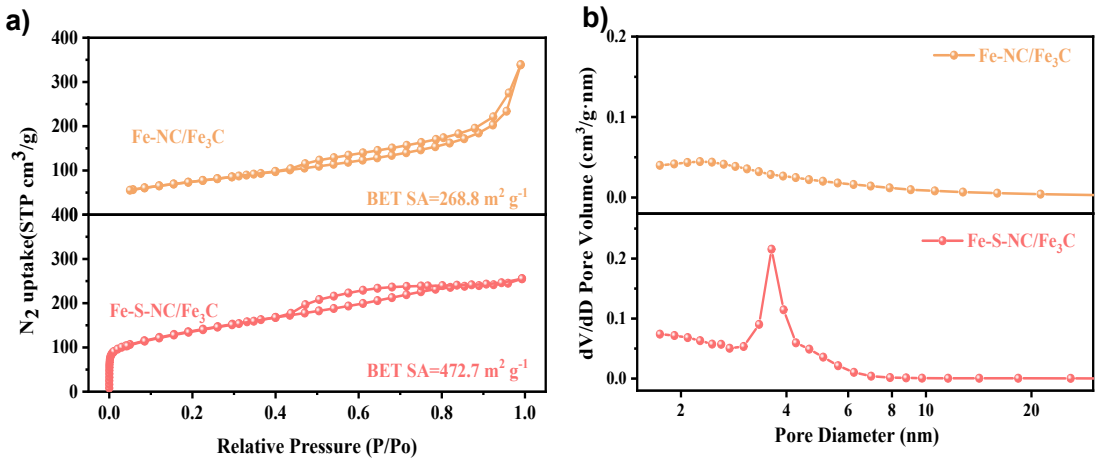

Figure S6. N_2 adsorption-desorption isotherms and pore size distributions of Fe-S-NC/Fe_3C and Fe-NC/Fe_3C.

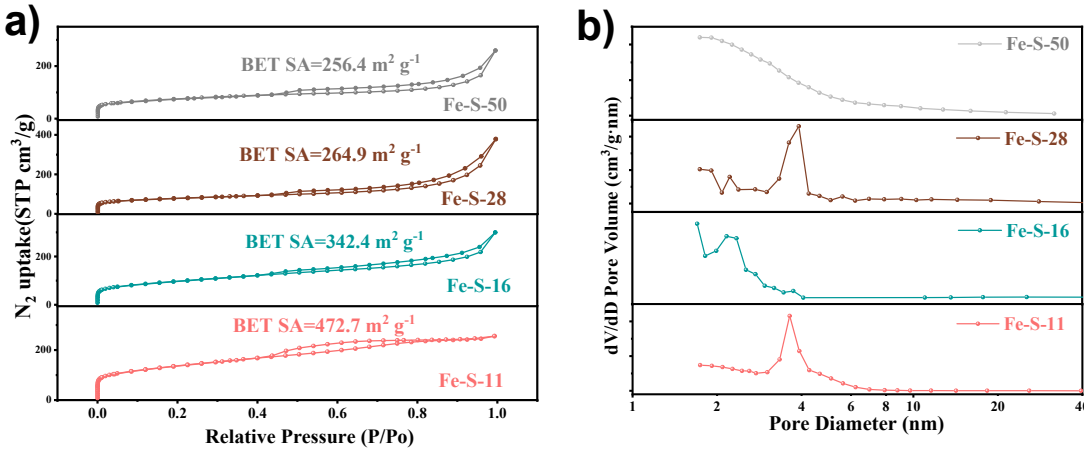

Figure S7. Powder N_2 adsorption/desorption isothermal curves and pore size distribution of Fe-S-X catalysts fabricated with different weight ratios of thiourea.

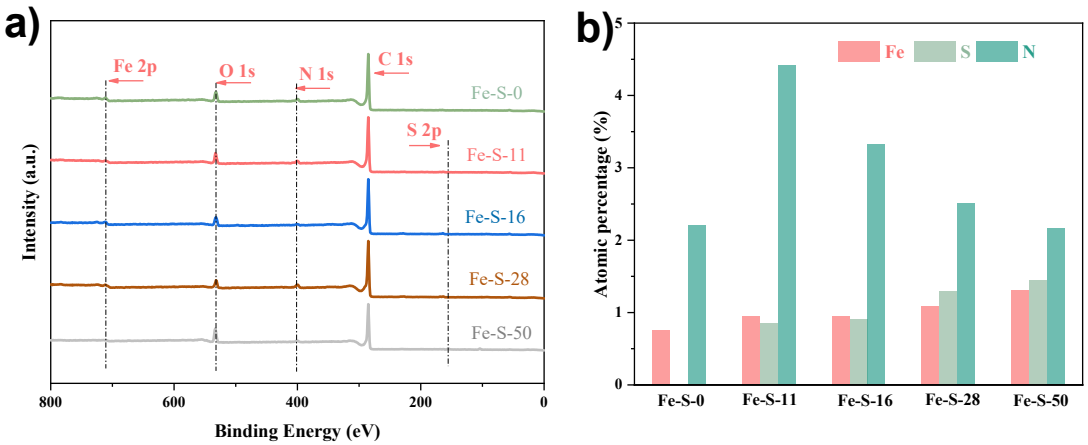

Figure S8. (a) XPS survey spectra of Fe-S-X catalysts prepared by different ratios of thiourea doping, and (b) their elemental content histograms.

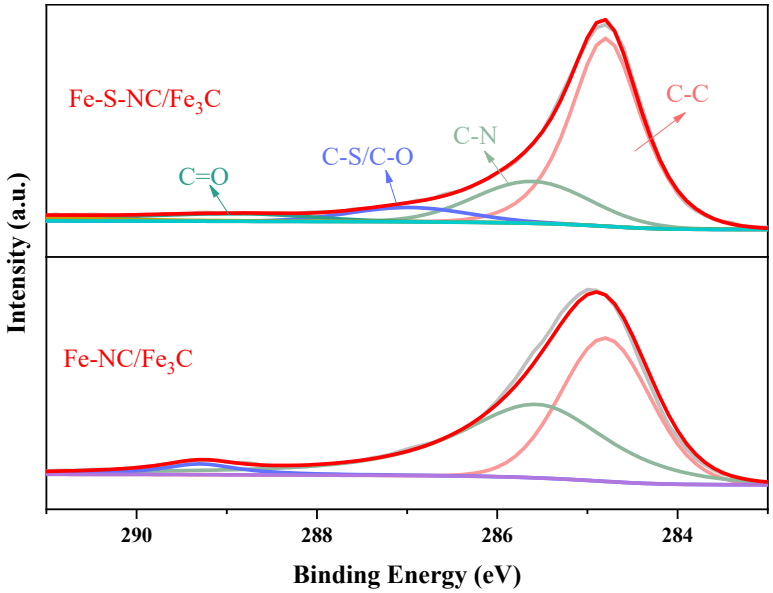

Figure S9. High-resolution XPS spectra of C 1s of Fe-S-NC/Fe_3C and Fe-NC/Fe_3C

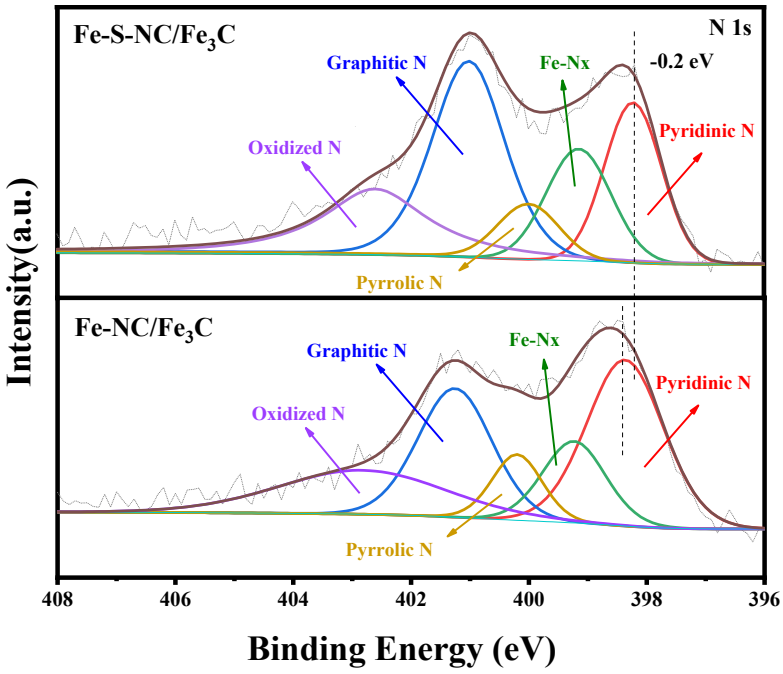

Figure S10. High-resolution XPS spectra of N 1s of Fe-S-NC/Fe_3C and Fe-NC/Fe_3C.

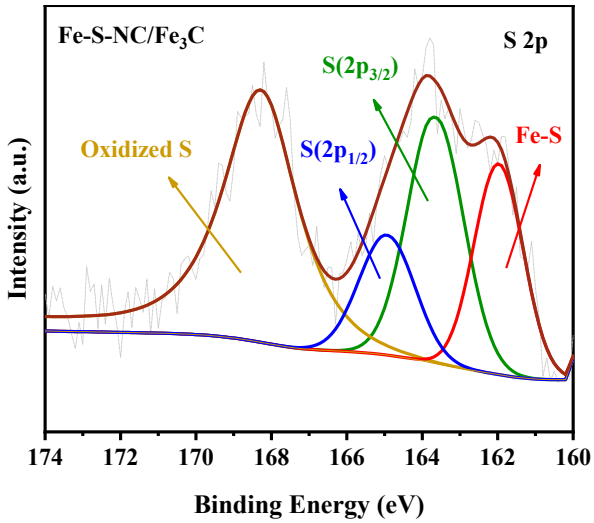

Figure S11. High-resolution XPS spectra of S 2p of Fe-S-NC/Fe_3C.

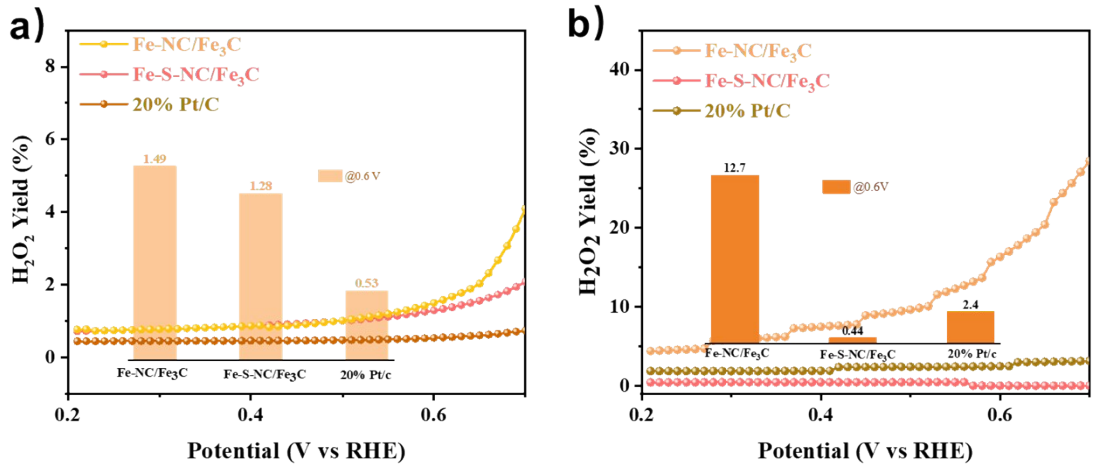

Figure S12. H_2O_2 yield in O_2-saturated 0.1M $HClO_4$ (a) and 0.1M KOH (b). The histogram inside is the H_2O_2 yield at 0.6 V of different catalysts.

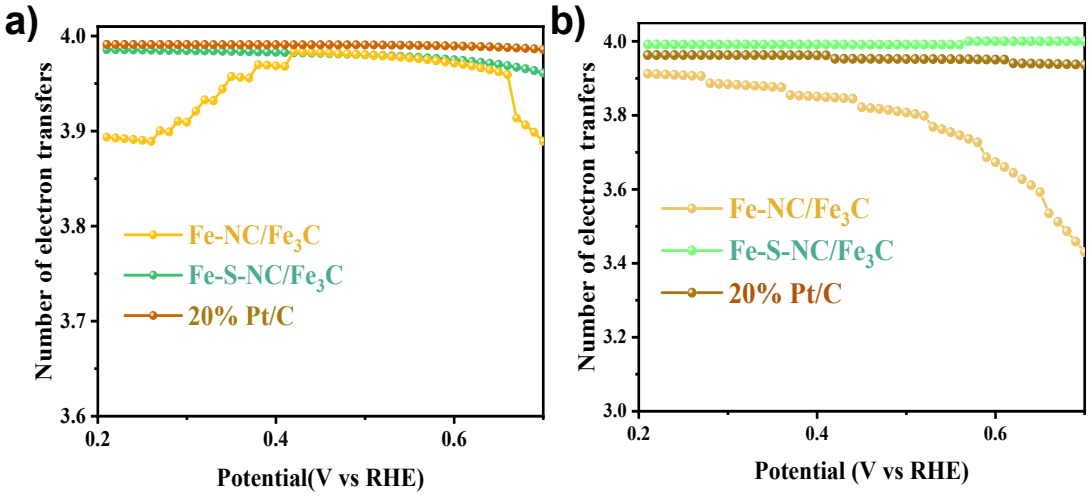

Figure S13. Electron transfer number in (a) 0.1 M $HClO_4$ and (b) KOH of different catalysts

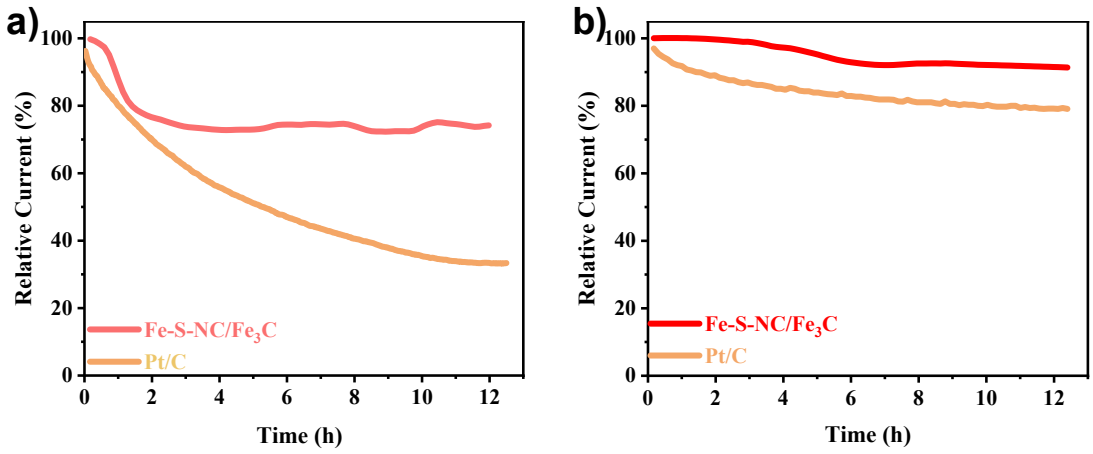

Figure S14. 12 h long discharge curves of Fe-S-NC/Fe_3C and 20% Pt/C in O_2-saturated a) 0.1 M $HClO_4$ and b) KOH at 0.6 V (vs RHE).

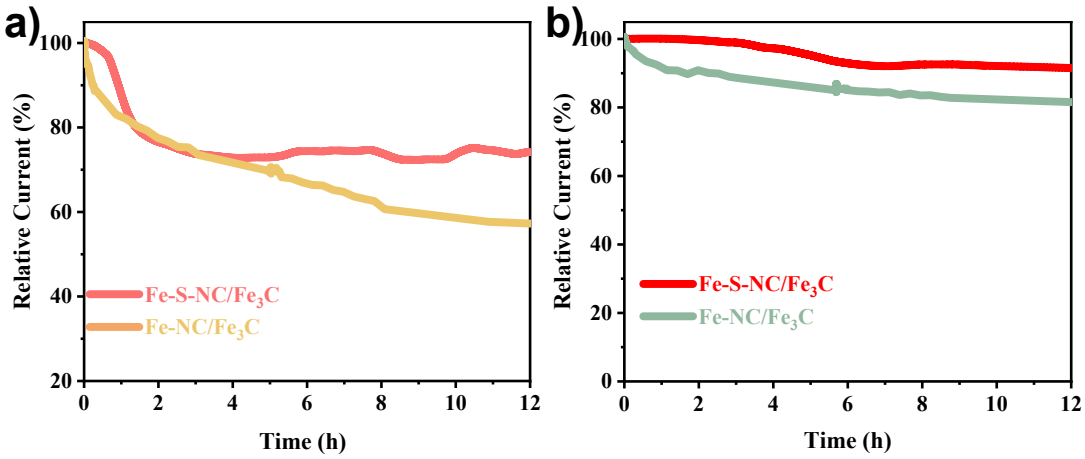

Figure S15. 12 h long discharge curves of Fe-NC/Fe_3C and Fe-S-NC/Fe_3C in O_2-saturated 0.1 M $HClO_4$ (a) and KOH(b) at 0.6 V (vs RHE).

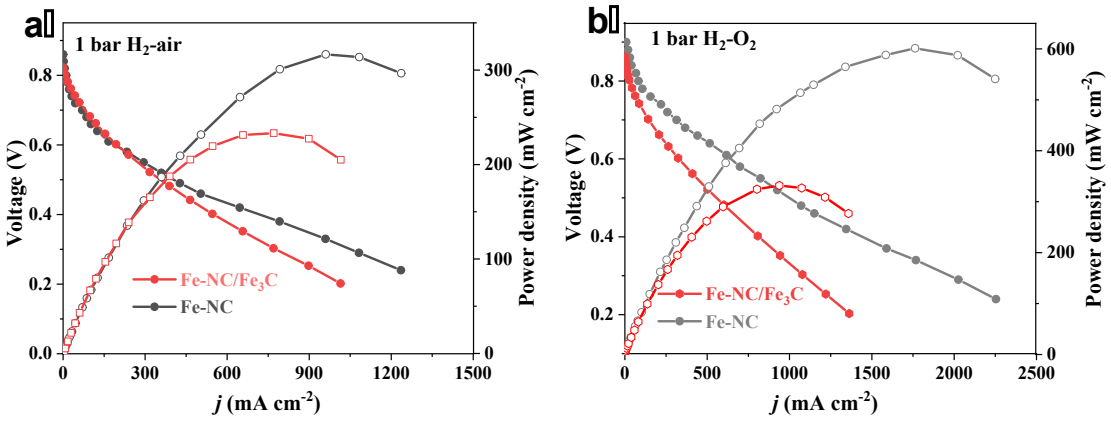

Figure S16. Single PEM fuel cell performance of Fe-NC/Fe_3C and Fe-NC as the cathode catalyst in conditions of (a)1 bar H_2/air and (b) 1 bar H_2/O_2.

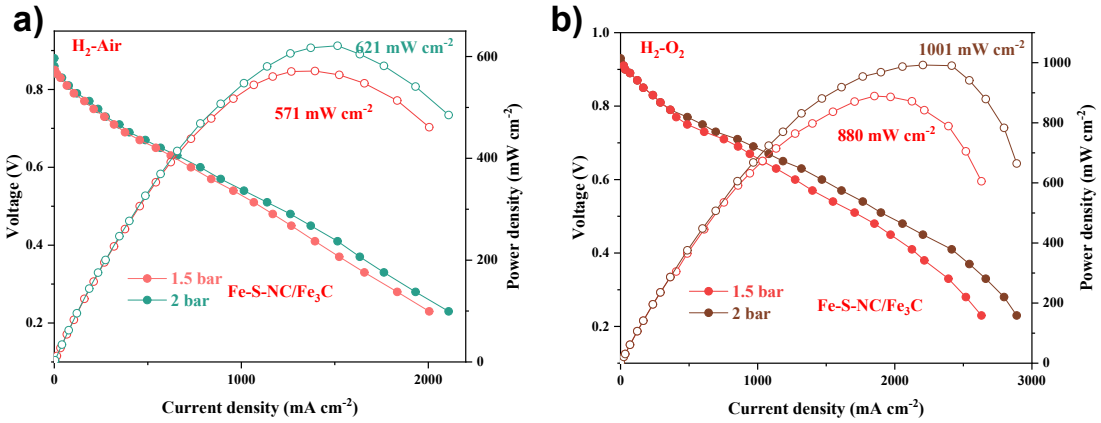

Figure S17. Performance of Fe-S-NC/Fe_3C as cathode catalysts in PEMFCs under (a) H_2/Air and (b) H_2/O_2 environments at back pressures of 1.5 and 2 bar.

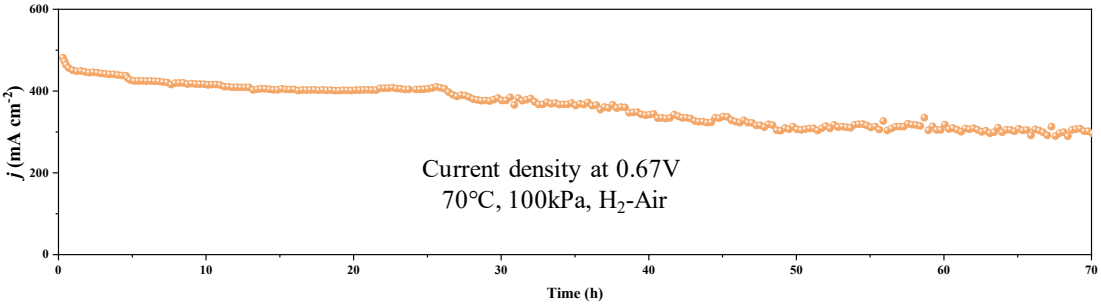

Figure S18. Fe-S-NC/Fe_3C as the cathode catalyst for long-time discharge in H_2/air.

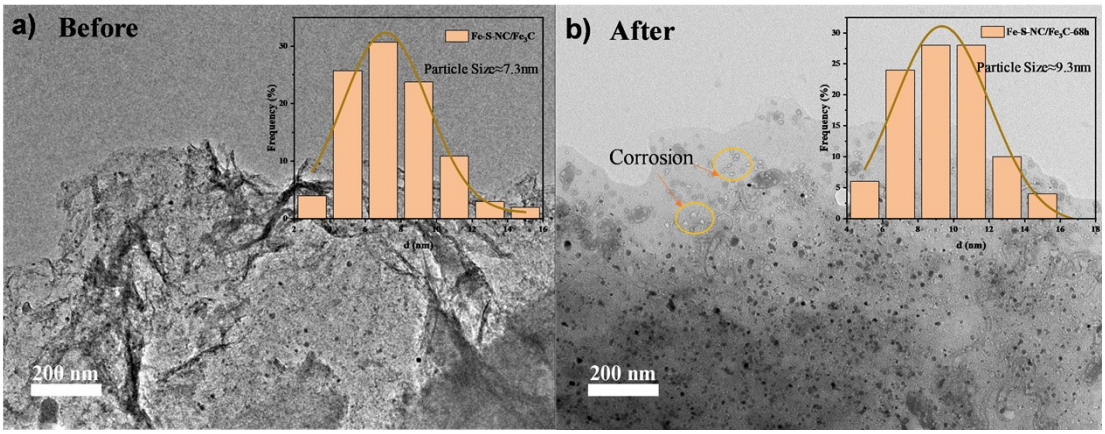

Figure S19. TEM images of Fe–S-NC/Fe_3C obtained before and after durability testing in MEA at a constant cell voltage of 0.67 V in 1 bar H_2-O_2.

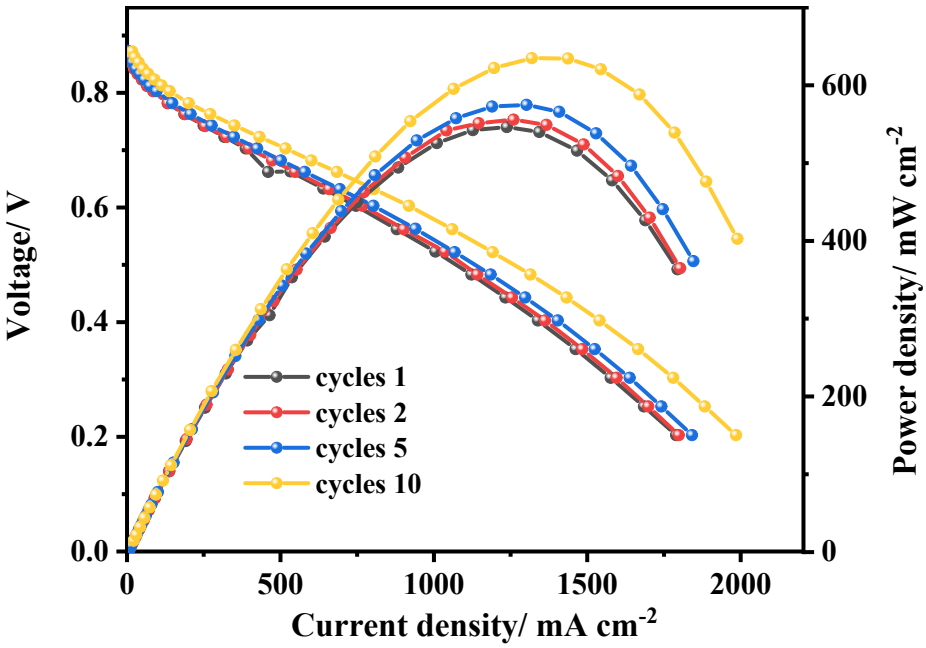

Figure S20. Polarization curves and power density of Fe-S-NC/Fe_3C from the 1st to 10th cycle after a long discharge.

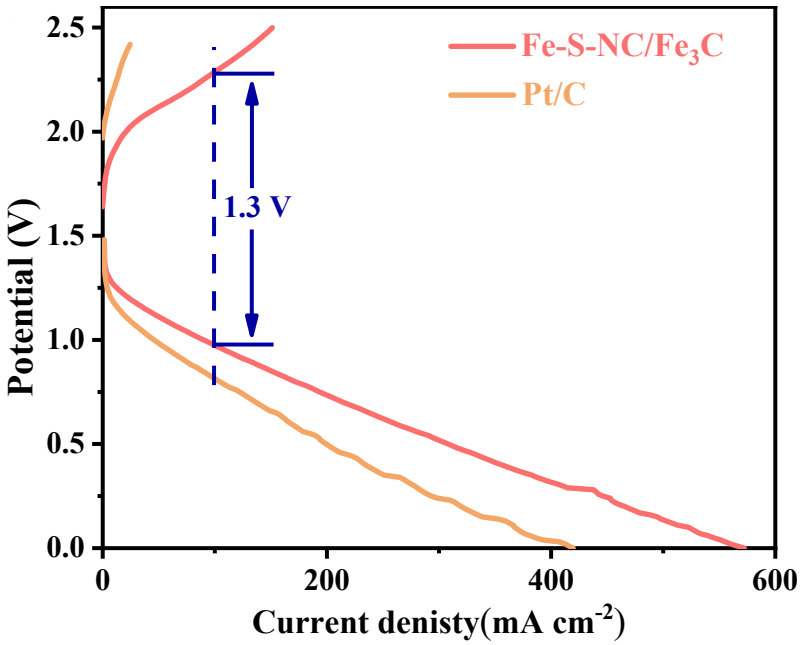

Figure S21. Charge and discharge polarization curves for Fe-S-NC/Fe_3C and Pt/C in Zn-air batteries.

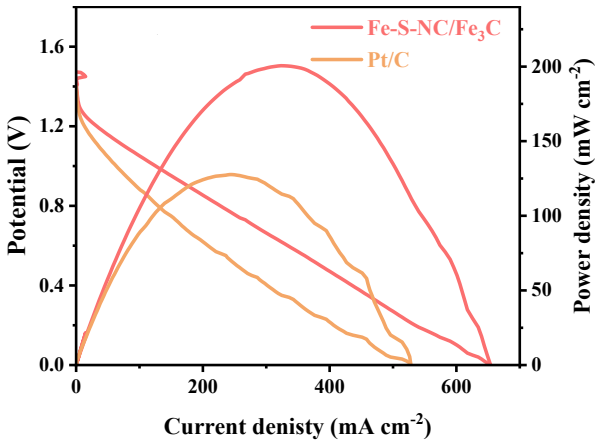

Figure S22. The polarization and power density curves of Fe-S-NC/Fe_3C and Pt/C in Zn-air batteries.

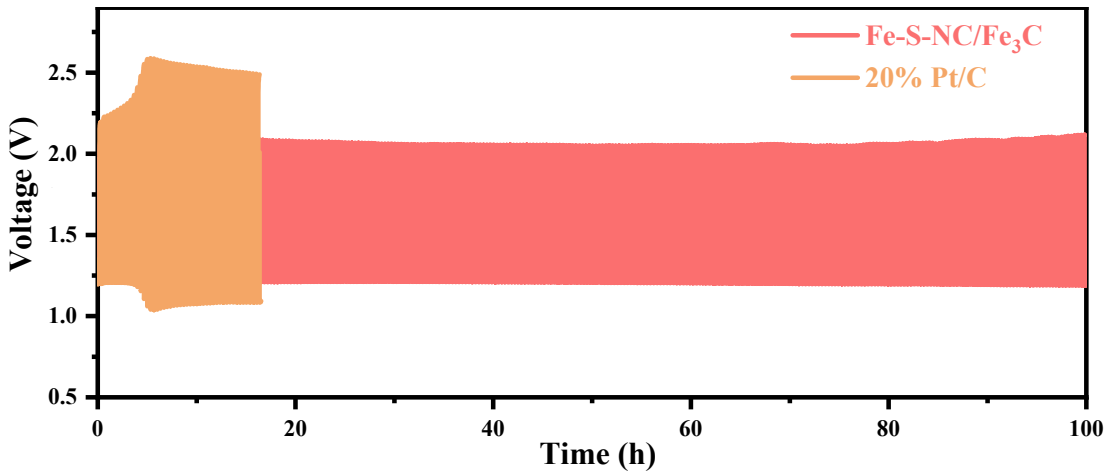

Figure S23. The constant current cycling performance at 5 mA cm^{-2} for Fe-S-NC/Fe_3C and Pt/C in Zn-air batteries.

.

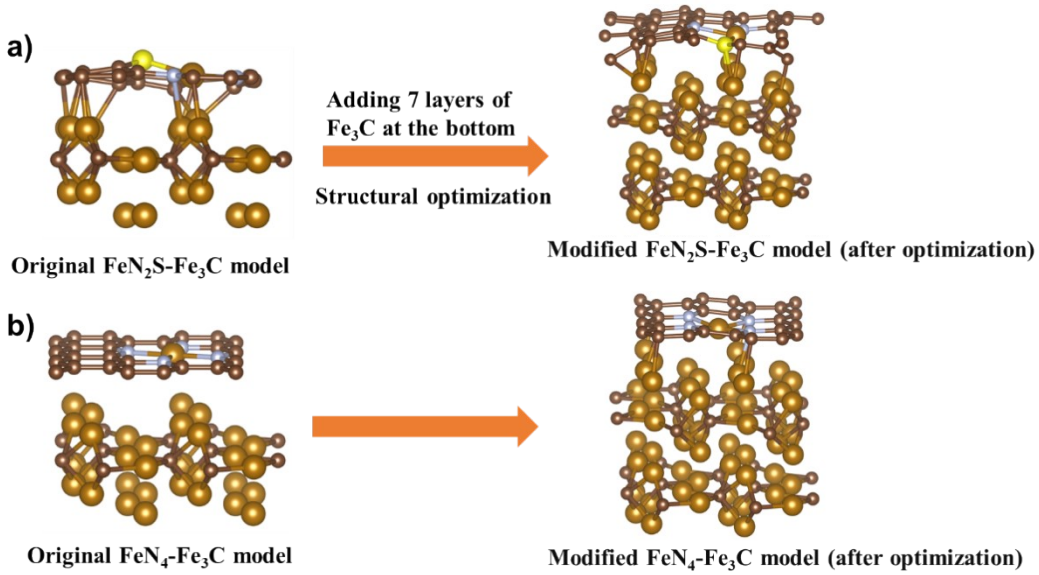

Figure S24. Models of Fe-S-NC/Fe_3C and Fe- NC/Fe_3C before and after optimization.

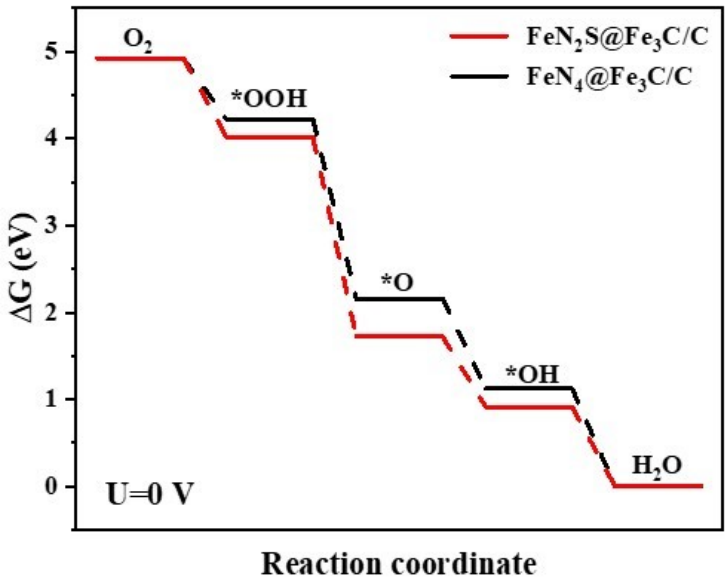

Figure S25. Free energy diagram of the reduction of O_2 to H_2O on FeN_2S/Fe_3C and FeN_4/Fe_3C under a potential of 0 V.

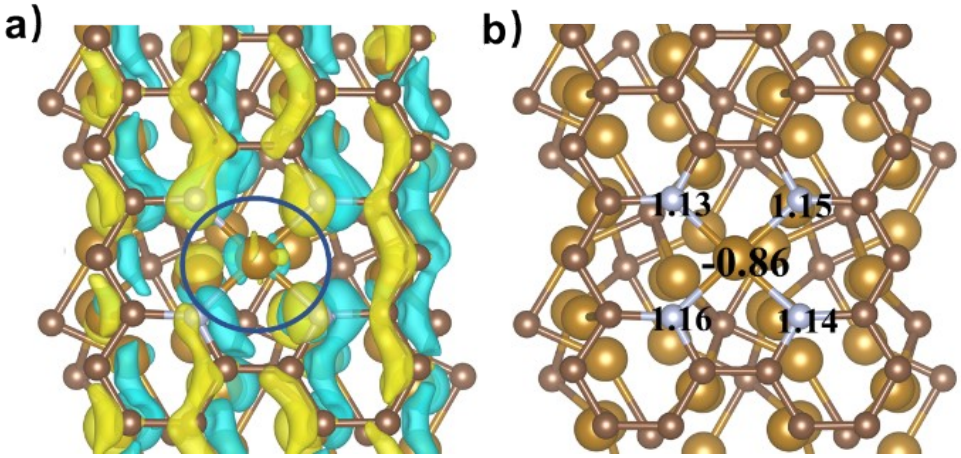

Figure S26. The charge density (a) and Bader charge distribution (b) in FeN_4/Fe_3C, with the yellow area representing the charge density increase and the light blue area representing the charge density decrease.

Table S1. Specific surface area, maximum pore volume and mesoporosity of the samples

Sample	**BET SA ($m^2 \cdot g^{-1}$)**	**V_{max} ($cm^3\ g^{-1}$)**	**Mesoporosity (%)**
Fe-S-0	268.8	0.10	90.9
Fe-S-11	472.7	0.792	92.6
Fe-S-16	342.4	0.195	90.5
Fe-S-28	264.9	0.360	89.73
Fe-S-50	256.4	0.115	66.6

Table S2. Elemental percentages in various Fe-S-X catalysts.

Sample	Fe (at. %)	S (at. %)	N (at. %)	C (at. %)
Fe-S-0	0.76	-	2.2	97.04
Fe-S-11	0.94	0.85	4.41	93.7
Fe-S-16	0.95	0.9	3.32	94.83
Fe-S-28	1.09	1.29	2.51	95.11
Fe-S-50	1.31	1.45	2.16	95.08

Table S3. Fraction of the different Fe species present in Fe-NC/Fe_3C and Fe-S-NC/Fe_3C

Sample	**Fe^0 (at%)**	**Fe^{2+} $2p_{3/2}$ (at%)**	**Fe-N (at%)**	**Fe^{3+} $2p_{3/2}$ (at%)**	**Fe^{2+} $2p_{1/2}$ (at%)**	**Fe^{3+} $2p_{1/2}$ (at%)**
Fe-NC /Fe_3C	8.7	16.5	25.3	16.5	9.7	23.3
Fe-S-NC /Fe_3C	24.4	8.5	26.8	6.2	25.6	8.5

Table S4. Fraction of the different N species present in Fe-NC/Fe_3C and Fe-S-NC/Fe_3C

Sample	Pyridinic-N (at%)	Fe-N_x (at%)	Pyrrolic-N (at%)	Graphitic-N (at%)	Oxidized-N (at%)
Fe-NC /Fe_3C	28.7	11.5	20.7	26.8	13.3
Fe-S-NC /Fe_3C	30.4	15.9	12.0	29.1	12.6

Table S5. EXAFS fitting parameters at the Fe K-edge for various samples（S_0^2=0.76）

Sample	shell	CN	R(Å)	σ^2	ΔE_0	R factor
Fe foil	Fe-Fe	8	2.47±0.01	0.0050	7.0±1.0	0.0033
	Fe-Fe	6	2.85±0.01	0.0064		
Fe-S-NC /Fe_3C	Fe-N	1.8±0.3	1.99±0.03	0.0068	4.4±3.2	0.0068
	Fe-S	0.8±0.1	2.27±0.02	0.0024		
	Fe-Fe	1.4±0.2	2.58±0.02	0.0060		

[a]*N*: coordination numbers; [b]*R*: bond distance; [c]σ^2: Debye-Waller factors; [d] ΔE_0: the inner potential correction. *R* factor: goodness of fit.

Table S6. Comparison of H_2−air fuel cell performance of Fe-S-NC/Fe_3C materials with published M-N-C catalysts

Catalyst	P_{max} (W cm^{-2})	H_2/air Flow Rate (sccm)	Abs Pressure (bar)	Loading (mg cm^{-2})	Year	References
Fe-S-NC /Fe_3C	0.535	400/600	1	3	2024	**This work**
Fe–NC/Sca^{ad}-^{CeO2}	0.401	300/400	2	4	2023	[1]
Fe-SAC-MOF-5	0.31	---	1	4	2022	[2]
d-SA-FeNC	0.502	500/1000	1	1	2022	[3]
Fe-N-C-SP	0.43	300/500	1	4	2022	[4]
FeNC-CVD-750	0.37	500/2000	1	6	2021	[5]
Fe/NC-NaCl	0.39	150/200	1	4	2021	[6]
Fe-N-C/MA-200	0.47	200/200	1	3	2021	[7]
Fe/N/C(4mlm)-OAc	0.436	300/300	1	3	2020	[8]
Co(mIm)-NC(1.0)	0.32	---	1	6.3	2020	[9]
$FeCl_2$-NC-1000	0.28	200/1000	1	4	2020	[10]
FeN4/HOPC-c-1000	0.42	200/300	1	4	2020	[11]
C-FeZIF-1.44-950	0.463	300/300	~2	1	2019	[12]
TPI@Z8(SiO_2)-650-C	0.42	300/500	1	2	2019	[13]
ZIF-NC-0.5Fe-700	0.32	200/200	1	3.5	2019	[14]
1.5Fe-ZIF	0.36	200/200	1	4	2019	[15]
FeN_x/GM	0.43	300/300	1.4	4	2019	[16]

Table S7. The ICP content of Fe element in Fe-S-NC/Fe_3C catalyst before and after the long-term discharge test in 1 bar H_2-O_2.

Simple	Fe (wt. %)	Retention rate
Before	18.5	100%
After	14.67	79.3%

Table S8. Gibbs free energy for ORR reaction steps of catalysts with different configurations

U=0V/1.23V	FeN_4/Fe_3C	FeN_2S/Fe_3C
ΔG1	−1.27/−0.53	−1.11/0.32
ΔG2	−1.98/−0.83	−2.13/−1.05
ΔG3	−1.09/0.2	−0.92/0.41
ΔG4	−0.58/0.1	−0.76/0.31

References:

1 X.-Y. Cheng, X.-T. Jiang, S.-H. Yin, L.-F. Ji, Y.-N. Yan, G. Li, R. Huang, C.-T. Wang, H.-G. Liao, Y.-X. Jiang et al., *Angew. Chem. Int. Ed.* **2023**, e202306166.

2 X. Xie, L. Shang, X. Xiong, R. Shi, T. Zhang, *Adv. Energy Mater.* **2022**, *12*, 2102688.

3 L. Shi, X. Lin, F. Liu, Y. Long, R. Cheng, C. Tan, L. Yang, C. Hu, S. Zhao, D. Liu, *ACS Catal.* **2022**, *12*, 5397.

4 J. Zhu, Z. Fang, X. Yang, M. Chen, Z. Chen, F. Qiu, M. Wang, P. Liu, Q. Xu, X. Zhuang et al., *ACS Catal.* **2022**, *12*, 6409.

5 L. Jiao, J. Li, L. L. Richard, Q. Sun, T. Stracensky, E. Liu, M. T. Sougrati, Z. Zhao, F. Yang, S. Zhong et al., *Nat. Mater.* **2021**, *20*, 1385.

6 Q. Wang, Y. Yang, F. Sun, G. Chen, J. Wang, L. Peng, W.-T. Chen, L. Shang, J. Zhao, D. Sun-Waterhouse et al., *Adv. Energy Mater.* **2021**, *11*, 1000687.

7 Y. Zhou, G. Chen, Q. Wang, D. Wang, X. Tao, T. Zhang, X. Feng, K. Müllen, *Adv Funct. Mater.* **2021**, *31*, 2102420.

8 Y. Li, P. Zhang, L. Wan, Y. Zheng, X. Qu, H. Zhang, Y. Wang, K. Zaghib, J. Yuan, S. Sun et al., *Adv. Funct. Mater.* **2021**, 31, 2009645.

9 X. Xie, C. He, B. Li, Y. He, D. A. Cullen, E. C. Wegener, A. J. Kropf, U. Martinez, Y. Cheng, M. H. Engelhard et al., *Nat. Catal.* **2020**, *3*, 1044.

10 J. Li, L. Jiao, E. Wegener, L. L. Richard, E. Liu, A. Zitolo, M. T. Sougrati, S. Mukerjee, Z. Zhao, Y. Huang et al., *J. Am. Chem. Soc.* **2020**, *142*, 1417.

11 M. Qiao, Y. Wang, Q. Wang, G. Hu, X. Mamat, S. Zhang, S. Wang, *Angew. Chem. Int. Ed.* **2020**, *132*, 2710.

12 Y. Deng, B. Chi, J. Li, G. Wang, L. Zheng, X. Shi, Z. Cui, L. Du, S. Liao, K. Zang et al., *Adv. Energy Mater.* **2019**, *9*, 1802856.

13 X. Wan, X. Liu, Y. Li, R. Yu, L. Zheng, W. Yan, H. Wang, M. Xu, J. Shui, *Nat. Catal.* **2019**, *2*, 259.

14 J. Li, H. Zhang, W. Samarakoon, W. Shan, D. A. Cullen, S. Karakalos, M. Chen, D. Gu, K. L. More, G. Wang et al., *Angew. Chem. Int. Ed.* **2019**, *58*, 18971.

15 H. Zhang, H. T. Chung, D. A. Cullen, S. Wagner, U. I. Kramm, K. L. More, P. Zelenay, G. Wu, *Energy Environ. Sci.* **2019**, *12*, 2548.

16 X. Fu, N. Li, B. Ren, G. Jiang, Y. Liu, F. M. Hassan, D. Su, J. Zhu, L. Yang, Z. Bai et al., *Adv. Energy Mater.* **2019**, 9, 1803737.